# ECOGENIC RESPONSE AND DOSIMETRIC EVALUATION OF HYDROXYAPATITE MACROAGGREGATES IMPLANTS

**Bruno M. Mendes**
**Tarcisio P.R. Campos**
Curso de Pós Graduação em Ciências e Técnicas Nucleares - CCTN/UFMG,
Av. Antônio Carlos, 6627, CEP: 31270901, Belo Horizonte, MG, Brasil,
campos@nuclear.ufmg.br

***ABSTRACT*** *Hydroxyapatite macroaggregates with incorporated radionuclides, namely M-HAP ("M"= metallic radionuclides such as: $^{89}Sr$, $^{90}Y$, $^{165}Dy$, $^{166}Ho$ or $^{188}Re$), present a great potential for brachytherapy implants. HAP is biocompatible, presenting neither local nor systemic toxicity and can incorporate radionuclides. In the present work, experimental models were used to study the spatial distribution, X-rays and ecogenic responses of M-HAP macroaggregates introduced by high viscosity carboxy-methyl-cellulose gel through interstitial implants into kidney, lung, liver, brain and muscle experimental samples. A Monte Carlo computational dosimetric evaluation of M-HAPs interstitial implants was also performed taken conventional $^{125}I$ seeds as comparison. The images demonstrated high ecogenicity and easy ultrasound identification in all evaluated tissues experimental models. A weak radiological response was verified in all X-ray images. The incorporation of high atomic number (Z) radionuclides to the hydroxyapatite structure may improve the X-rays contrast. The M-HAP macroaggregates presented suitable dose distribution for tumor control, matching radiodosimetric standard on oncology. Indeed, $^{188}Re$-HAP implants present radiodosimetric advantages when compared with $^{125}I$ seeds.*

**Keywords**: Dosimetry, radiotherapy implants, radiological response.

## 1. Introduction

Hdroxyapatite (HAP) is a non-toxic and non-immunogenic bioceramic (Manso et al, 2002). Studies report that in few milligrams it is easily absorbed by the organism (Andrade et al, 2002). HAP composition presents the chemical formula $Ca_{10}(PO_4)_6(OH)_2$; however, due to its peculiar structure, it can be considered as a solid solution and the Calcium atoms can be substituted by other cations, for example metallic radionuclides cations (Nadari et al, 2003). The synthesis of hydroxyapatite with metallic cations substituting the Calcium in its structure is also possible, avoiding the necessity of further replacements (Nadari et al, 2003). Such features evidence a great potential to the radionuclide incorporated hydroxyapatite macroaggregate M-HAP (where M is a suitable metallic radionuclide) in brachytherapy implants.

Metallic encapsulated $^{125}I$ and $^{103}Pd$ seeds implants occur in the practical clinic for central nervous system (CNS) and prostatic tumor treatments (Laperriere et al, 1998) (Pedley, 2002). Fluoroscopy and computerized tomography techniques are generally used in this seeds implantation and dosimetry. Those seeds present suitable spatial radiological identification due to a metal inert core (Ulin et al, 1997). The presence of calcium and β-emitters radionuclides as $^{89}Sr$, $^{90}Y$, $^{165}Dy$, $^{166}Ho$, $^{153}Sm$ and $^{188}Re$ atoms in the HAP structure confer radiopacity to its macroaggregates; however due to the few mass content, localization by conventional X-rays modality is difficult. The possibility to incorporate inert agent for contrasting still exists. In this way, the current metallic seed implantation and dosimetry protocols could also be applied for the proposed (M-HAP) macroaggregates implant.

This work evaluates radiological and ecogenic response of Ca-HAP [HAP-91/JHS Chemical Laboratory] macroaggregate implants (with or without barium sulphate as X-ray contrast medium) in "*in vitro*" experimental models (EM). A comparative radiodosimetric analysis is presented considering $^{125}I$ seeds and M-HAP gel macroaggregates, in order to verify the clinical viability of applying these bioceramic materials. The theoretical methodology is based on the investigation of the specific energy deposition emitted by radionuclide-hydroxyapatite macroaggregate in deep brain interstitial implants through a stochastic computer code (MCNP4) and deterministic spatial dose distribution code, in-house made (Briesmeister, 1993).

## 2. Methods

### 2.1 Experimental Model (EM)

Acrylic boxes were set up with 15x 15 x "T" cm in which T is the EM thickness taken to the radiological study. The boxes had been filled with Agar base support medium, at the density of $1.01 g.cm^3$, due to its close radiological equivalence to human tissues. Previously to the medium solidification at laboratory temperature, animal model (pig) organs or organs fractions were added to each filled box (Fig.1), in such a way that the tissue homogeneously occupied more than 90% of the box volume. Such box has only one type of tissue. The liquid agar-type support medium gave support to the organ and removed the empty spaces, allowing the ultrasound transmission. Image will be severely blurred if air bubbles appear between the transducer and the organ. The following organs were evaluated: kidney, lung, liver, brain and muscle. They generated the setup model EM-kidney, EM-lung, EM-liver, EM-brain, EM-muscle, respectively

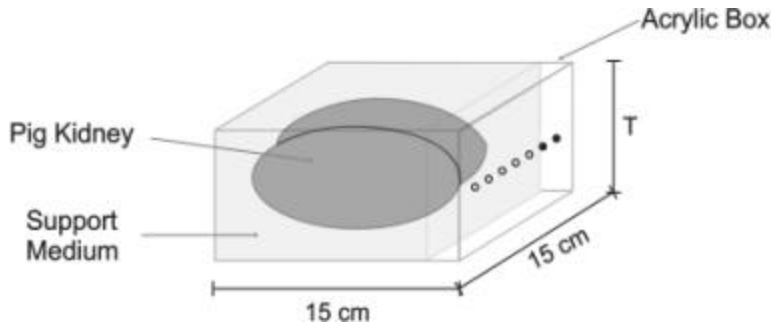


Figure 1- Schematic drawing of the animal sample placement into the acrylic box filed with radiological tissue equivalent support medium.

**2.2 Ca-HAP Macroaggregate Gel**

A high viscosity gel was previously prepared adding 0.1g of carboxy-methyl-cellulose (CMC) in 10 ml of water (medium A). The medium B was obtained by mixing 2.0 g of calcium hydroxyapatite [HAP-91/JHS Chemical Laboratory], in the size ranges of 90µm-150µm, with 3ml of medium A. The Ca-HAP macroaggregate gel contrast medium, namely medium C, was obtained by mixing 3 ml of CMC gel, 1.0 g of HAP-91 and 1.0 g of barium sulphate.

**2.3 Implants and Images**

Medium B and C were applied in the experimental models through a specific mechanical device, developed in the laboratory for such purpose, connected to a 0.6mm diameter needle. The medium B, without contrast, was applied in the EM-kidney, EM-brain, EM-muscle, EM-lung, EM-kidney, EM-liver experimental models. The Ca-HAP gel with the barium contrast, medium C, was implanted only in EM-lung and EM-kidney. After the needle application, a copper wire was fixed at the needle start position site to mark the position of the implants without contrast (medium B) at the radiological image. A 120 elements and 7.5 MHz frequency transducer was used in the ecographic evaluation. The X-ray equipment was set at the voltages of 40KV to 50 KV and 25mA to 50mA current in accordance to the thickness of the box used in the experimental model. Various radiological and ultrasound shots were obtained from the experimental models, with medium B and C implants.

**2.4 Radial Dose Profile (RDP) evaluation per unit of implant's segment**

The RDP evaluation for M-HAP segments implanted through radio-opaque viscous gel-type medium, and for individual $^{125}I$ seeds were obtained through computational modeling. M-HAPs constituted by $^{89}Sr$, $^{90}Y$, $^{165}Dy$, $^{166}Ho$ or $^{188}Re$ were investigated. Figure 2 illustrates the model adopted for the radial dose profile evaluation per source segment. A 0.6mm diameter and 30mm height cylinder positioned in a sphere center represents a unitary implant's segment. Concentric cylinders 5mm height, and with radius increments of 0.25mm were defined around the seed. The emitted particles were photons and electrons. The absorbed dose per transition (Gy/tr) was evaluated in each radial ring utilizing the nuclear code MCNP4. The sphere and the concentric cylinders were setup to be constituted by cerebral tissue (ICRU-46, 1992). The implant cylinder presents the M-HAP gel-type chemical composition. This composition varies as a function of the employed radionuclide. The particles emission was defined inside the central cylinder (M HAP gel-type). The $\beta$ particles, Auger electrons, $\gamma$ and X-ray energy and emission probabilities of each radionuclide decay was considered. A mathematical model was applied to discretely reconstruct the five radionuclides continuous beta emission spectra for MCNP code input.

**2.5 Bi-dimensional isodose curves for configurations of multiple implants**

Based on the RDP generated by each radionuclide, an "*in-house*" software generates the dose in a transversal plan considering the M-HAP segments and $^{125}I$ seeds distribution. Configurations with 4, 5 and 7 implanted segments were analyzed and 2D isodose curves were generated for each configuration looking for optimal segment arrangement determination, preserving greater tumor dose and avoiding hot spots at the implant region.

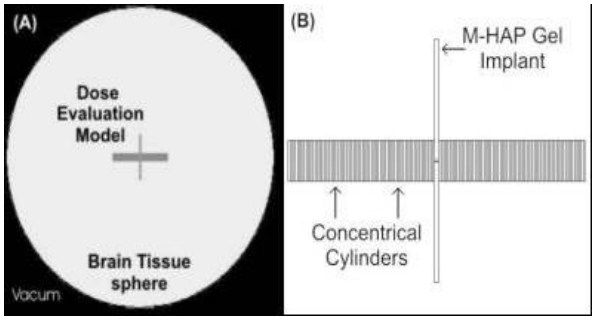


Figure 2 – (A) MCNP4 computational model used for RDP evaluation. (B) Central region zoom.

**2.6 Three-dimensional dose distribution from a M-HAP implant's configuration**

A brain computational phantom was developed to be executed by MCNP4 nuclear code, based on voxel model (Fig.3A). A 3.0 x 2.5 x 2.5 cm tumor in left brain hemisphere was simulated. $^{188}$Re-HAP cylindrical implants were placed inside de lesion site (Fig.3A). The distances between implanted segments and their number were previously defined. IMC6702 $^{125}$I seeds were setup following equivalent brain implant standards (Fig.3B).

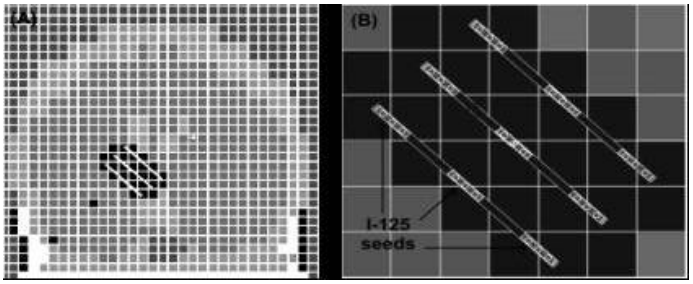


Figure 3 – (A) Voxel model coronal slice in tumor plane. Three M-HAP cylindrical implants can be observed.(B) $^{125}$I seeds placed at the model tumor.

**3. Results**

**3.1 X-ray response**

Radiological response of the implants into the EM-models filled with medium B and C can be observed in figures 4A and 4B. Recognition of tenuous lines in the medium B implant sites were possible in the radiological X-ray film at the EM-kidney and EM-muscle models (not shown), however for the other EM-models lines were not identified. After the X-ray film digitalization, only metallic wires can be depicted (fig. 4A). For medium C implants, even without the placement of the metallic wires in the needle start position, the placements in which medium C was applied were easily spotted at the tested EM-models (fig. 4B).

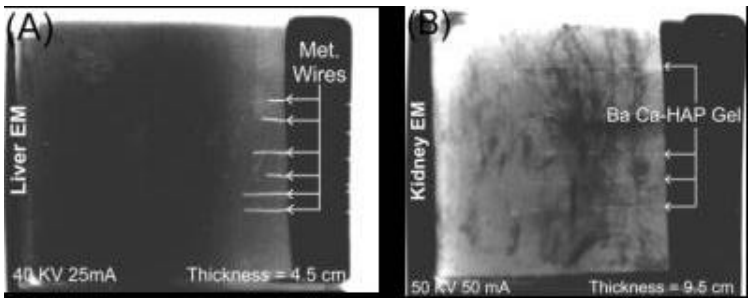


Figure 4 – Radiological response of Experimental Models (EM) implants. (a) digitalized image of the implants of the Ca-HAP Gel without contrast (medium B) in EM-liver. (b) digitalized image of the implants of Ca-HAP Gel with Barium contrast (medium C) in EM-kidney.

**3.2 Ecogenic response**

The Ca-HAP Gel ecographic response in two experimental models is shown in figure 5. The medium B and C presented high ecogenicity and notable visualization in all the soft tissues studied despite the thin diameter filled at the implants. The EM-muscle, EM-liver and EM-brain models presented suitable ecographic identification. However, EM-brain presents large amount of noise, worse response. Reverberation was identified due the inherent characteristic of the box used for the model.

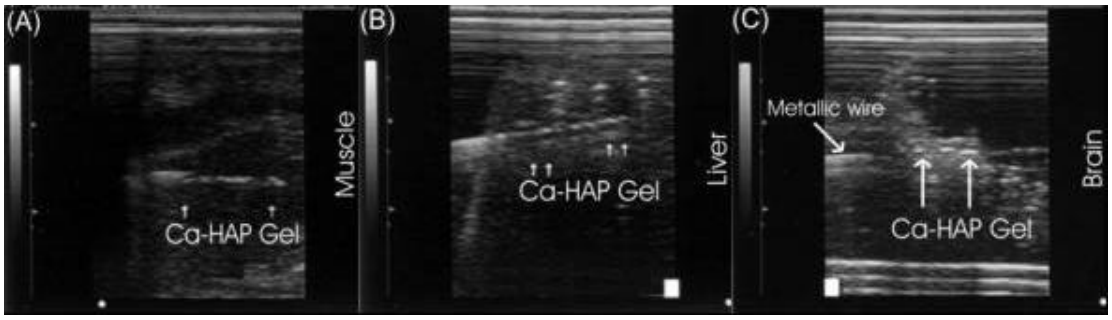


Figure 5 – Ecographic response of the Ca-HAP Gel without contrast in EM-liver (A), EM-muscle (B) and EM-brain (C) experimental models, based on a 120 elements and 7,5 MHz transducer.

**3.3 Radial Dose Profile (RDP)**

The RPD per transition are presented in Figure 6. The tissue's absorbed dose for β-emitters presents profiles that diminish smoothly with the increment of the radial distance, characterizing a plateau at a log x log plot. An abrupt fall occurs after this plateau. For $^{125}$I the dose falls exponentially, obeying the physical characteristics of the gamma-rays interaction with matter. The $^{90}$Y and the $^{188}$Re, β-emitters, with maximum energy over 2MeV, presented RDP per transition with lager plateaux, reaching up to 7-9 mm brain tissue-depth, which allow larger distance between segments. Besides, $^{188}$Re emits γ and X-rays that helps monitoring leakage or absorption after implantation. The $^{188}$Re half-life is 17 hours, so 90% of the total dose is delivered up to 22 hours. After 2 days, its activity will be decreased to insignificant levels, permitting bio absorption and infiltration phenomena. Natural rhenium should be selected for the subsequent studies due to its capability to monitoring implants through $^{186}$ Re cintilographic image.

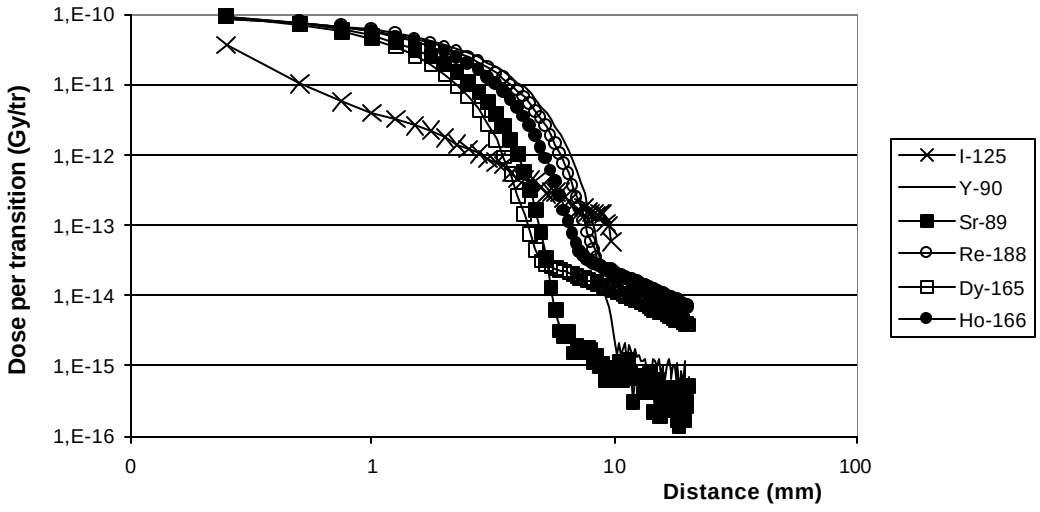


Figure 6 – Absorbed dose per transition as function of the radial distance, in a log x log graphic, for $^{90}$Y, $^{89}$Sr, $^{188}$Re, $^{165}$Dy, $^{166}$Ho – HAP gel-type and I-125 seed. The statistical errors were less than 5% except for $^{89}$Sr and $^{90}$Y in radius greater than 8mm.

### 3.4 Bi-dimensional isodose curves from multiple segment implants

The figure 7 presents the percentage isodose curves for two distinct spatial configurations of $^{125}$I seeds and $^{188}$Re-HAP type gel segments. $^{188}$Re-HAP segments present isodose curves more uniformly distributed, establishing that the tumor doses varies from 100% to 10% of maximum tumor dose (MTD) (10x) and, at the same time, the dose in healthy adjacent tissue falls from 10% to 1% of MTD in 2 mm, approximately. For the $^{125}$I the tumor doses vary from 100% to 1% of MTD (100x).

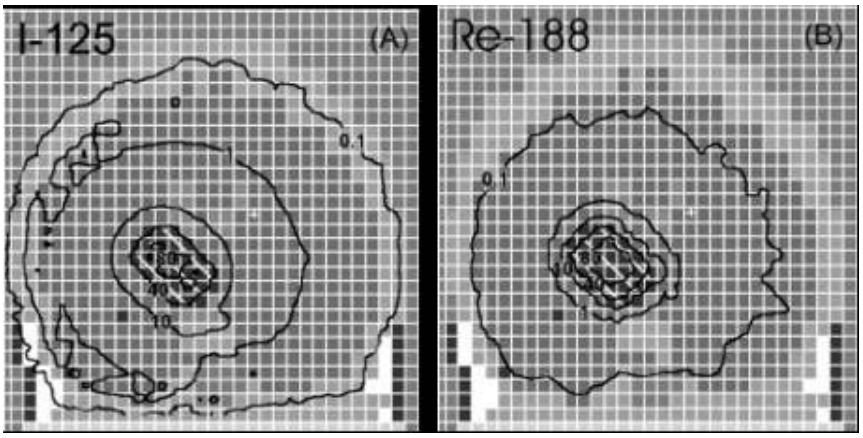


Figure 7- Absorbed Dose bi-dimensional isodose curves (percentage of MTD) obtained for two distinct 188Re-HAP gel-type segment's implants and 125I seeds configurations.

### 3.5 Three-dimensional dose distribution in a head phantom

The Re-HAP get-type and $^{125}$I seeds arrangements depicted in Fig. 7C and D were simulated in a computational phantom, with anthropomorphic and anthropometric equivalences to a human head. Observing the isodose configurations (Fig.8) it is noted that $^{125}$I and $^{188}$Re presented adequate tumor dose distribution. However, healthy tissues receive smaller doses when $^{188}$Re-HAP gel was applied instead of iodine seeds.

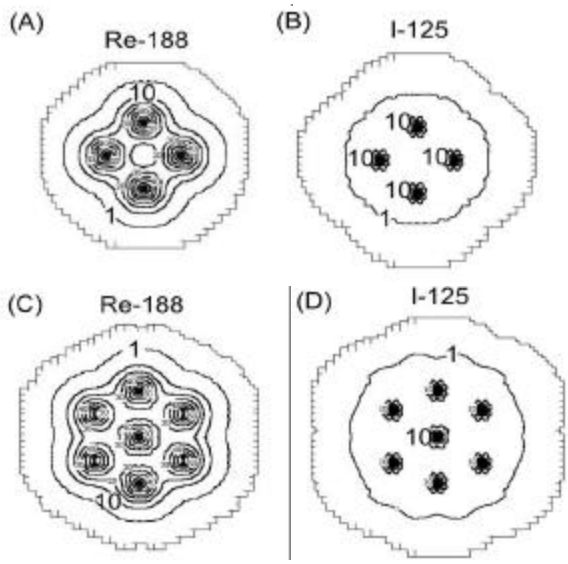


Figure 8 – Computational three-dimensional isodoses distribution for $^{125}$I seeds (A) and $^{188}$Re-HAP gel-type implants (B), at an anthropometrics and anthropomorphic head phantom, in function of the maximum tumor dose (MTD): The $^{125}$I maximum dose (100%) was 1.72 $10^{-13}$ Gy/tr and 6.42 $10^{-11}$ Gy/tr for $^{188}$Re-HAP.

## 4. Discussion

Despite the calcium presence, the medium B cannot be easily identified in x-ray images. The thin diameter of the implantations (0.6mm), few mass amounts, and the low atomic number of the macroaggregate atoms, plus 12cm tissue size are the main causes for the low radiological contrast. The implants of the medium C, using the Barium contrast, present suitable radiological identification in the EM-model tested. The high atomic number radionuclides as $^{89}$Sr, $^{90}$Y, $^{165}$Dy, $^{166}$Ho and $^{188}$Re present in the M-HAP structure will improve radiological X-ray contrast.

The medium B and C were fully identified in the five EM-models through ultrasound images. EM-brain had abnormal ecogenic response but the implants were still visible. Two factors contributed to the noise in EM-brain: i) the presence of air bubbles in support Agar medium between the organ fragments; and ii) the larger reverberation phenomena produced by the plane faces of the EM acrylic box. Reverberation in base and in top of the image can be seen (fig. 5C).

The Radial Dose Profile evaluation demonstrates the β-emitters "*plateau - abrupt fall*" behavior (fig. 6). Such behavior is very interesting in brachytherapy, since it permits large doses uniformly distributed in target volume, preserving adjacent healthy tissue. On the other hand $^{125}$I generates extremely high doses close to the seeds walls dropping by a $e^{(-\mu r)}$ factor with radial distance (Ulin et al, 1997).

The 2D isodose curves from multiple segments implants (fig. 7) illustrate that $^{188}$Re-HAP implants present better dose uniformity (100 - 10 % MTD) than $^{125}$I seeds (100 - 1 % MTD).

The 3D dose distribution evaluation in a computational head phantom shows that $^{125}$I and $^{188}$Re presented suitable tumor dose distribution. However, the geometry of the phantom voxels (5x5x5mm) was not enough, essentially in the implant/seed proximities, for reveling the dosimetric details. Mainly for the $^{125}$I case, hot spots were not identified.

## 5. Conclusions

In the *in vitro* experimental models, Ca-HAP Gel macroaggregate presented ecographics properties that allow spatial distinguishing of the implants into the all studied soft-organs tissue. The barium contrast supplement to the compound (medium C) allowed a good radiological X-ray identification. Hydroxyapatites containing high atomic number radionuclides as $^{89}$Sr, $^{90}$Y, $^{165}$Dy, $^{166}$Ho, $^{188}$Re and $^{153}$Sm substituting calcium atoms in its structure probably will improve contrast in CT and X-ray images, conditioning to a KV and mA adjustments. Future work will address the reduction of barium concentration. Still, the β-emitters addressed also emits γ rays and soft X-rays allowing the spatial biodistribution monitoring through gamma camera and SPECT – Single Photon Emission Computerizing Tomography

The techniques of fluoroscopy and CT clinically employed in $^{125}$I and $^{103}$Pd seeds implantation and post-implant dosimetry also can be used for M-HAP gel macroaggregates implants. Moreover, real-time implant procedures guided by ultrasound can be carried through for M-HAP gel in clinical practice. The main clinical features are simple technique, easy handling, low cost, precise spatial positioning, and non-visible collateral effects.

$^{188}$Re-HAP gel-type implants present radiodosimetric advantages when compared with $^{125}$I seeds, such as: i) limited dose fluctuations into the implant region which reduces the risk of sub-dosage or hot spots at tumor; ii) absolute value of MTD per transition a hundred times greater than $^{125}$I one, that allows the utilization of seeds with activity 100 times lower; iii) depletion of the absorbed dose forward to normal tissue falls to 1% after 7 mm from tumor region, reducing healthy tissue damage.

Future work will address detailed evaluations of the other M-type HAP compounds and "*in vitro*" and "*in vivo*" studies.

## 6. References


Andrade, A.L., Borges, A.P.B., Bicalho, S.M.C.M. "HAP-91 Síntese, Caracterização, Testes e Aplicações". JHS Laboratório Químico Ltda, 2001.

Briesmeister, J.F. "MCNP – A General Monte Carlo N - Particle Transport Code System". Version 4A, Los Alamos National Laboratory, 1993.

ICRU-46, "Report 46", International Commission on Radiation Units and Measurements, Bethesda, 1992.

Nadari, T., Hamdi, B., Savariault, J.M., Feki, H.E., Salah, A.B. "Substitution mechanism of alkali metals for strontium in strontium hydroxyapatite". Materials Research Bulletin. Vol. 38, p. 221-230, 2003.

Laperriere, N.J., Leung, P.M.K., Mckenzie, S., Milosevic, M., Wong, S., Glen, J., Pintilie, M., Bernstein, M. "Randomized study of brachytherapy in the initial management of patients with malignant astrocitoma". International Journal of Radiation Oncology Biology Physics. Vol. 41, p. 1005-1011, 1998.

Manso, M., Ogueta, S., Herrero-Fernández, P., Vazquez, L., Langlet, M., García-Ruiz, J. P. "Biological evaluation of aerosol-gel-derived hydroxyapatite coatings with human mesenchymal steem cells". Biomaterials. Vol. 23, p. 3985-3990, 2002.

Pedley, I.D. "Transperineal interstitial permanent prostate brachytherapy for carcinoma of the prostate". Surgical Oncology. Vol. 11, p.25-34, 2002.

Ulin, K., Bornstein, L.E., Ling, M.N., Saris, S., Wu, J.K., Curran, B.H., Wazer, D.E. "A technique for accurate planning of stereotactic brain implants prior to head ring fixation". International Journal of Radiation Oncology Biology Physics. Vol. 39, p. 757-767, 1997.

**8. Responsibility notice**

The author(s) is (are) the only responsible for the printed material included in this paper.